JOURNAL OF CATALYSIS 151, 135–146 (1995)

Delaminated Fe_2O_3–Pillared Clay: Its Preparation, Characterization, and Activities for Selective Catalytic Reduction of NO by NH_3

J. P. Chen, M. C. Hausladen, and R. T. Yang[1]

Department of Chemical Engineering, State University of New York at Buffalo, Buffalo, New York 14260

Received February 23, 1994; revised August 26, 1994

A delaminated Fe_2O_3–pillared clay catalyst was prepared for the selective catalytic reduction (SCR) of NO by NH_3 at above 300°C. The delaminated pillared clay was characterized by inductively coupled plasma–atomic emission spectroscopy chemical analysis, X-ray diffraction structure and line broadening analyses, micropore size probing, and Mössbauer analysis. These analyses showed that the catalyst contained fragmented Fe_2O_3–pillared clay forming "house-of-cards" structure with dispersed Fe_2O_3 particles approximately 170 Å in size. The SCR activity of the delaminated pillared clay was higher than the commercial-type V_2O_5 + WO_3/TiO_2 catalyst, and also higher than the undelaminated pillared clay and supported Fe_2O_3 catalysts, under conditions without SO_2. Infrared measurements of adsorbed NH_3 showed strong Brønsted acidity which was caused possibly by interactions between Fe_2O_3 and clay.

INTRODUCTION

Selective catalytic reduction (SCR) of nitrogen oxides with ammonia is of increasing industrial importance. A comprehensive review of the subject is available (1). The commercial catalysts are V_2O_5 with mixed WO_3 and/or MoO_3 supported on TiO_2. A direct correlation between the SCR activity and the Brønsted acidity of V_2O_5 has been observed (2–5), and the Brønsted acid sites are thought to be the active sites. Besides V_2O_5, a large number of catalysts have activities for the SCR reaction, some of which have also been reviewed. First results of SCR activities on pillared clays and potential advantages of using pillared clays have been reported by Yang *et al.* (6).

Pillared interlayered clays (PILC), or pillared clays, are two-dimensional zeolite-like materials prepared by exchanging the charge-compensating cations between the clay layers with large inorganic hydroxycations, which are polymeric or oligomeric hydroxy metal cations formed by hydrolysis of metal oxides or salts. Upon heating, the metal hydroxycations undergo dehydration and dehydroxylation, forming stable metal oxide clusters which act as pillars keeping the silicate layers separated, creating interlayer space (gallery) of molecular dimensions. Much interest and research have been directed to metal oxide PILC since their first successful syntheses in late 1970s (7–11). Comprehensive reviews of the voluminous literature on the subject are available (12–14). In principle, any metal oxide or salt that forms polynuclear species upon hydrolysis (15) can be inserted as pillars, and all layered clays of the abundant phyllosilicate family as well as other layered clays can be used as the hosts (references cited in 13, and 16–18). Because of its large pores and hydrothermal stability (to 700°C), the main early interest in PILC was in the possibility of replacing zeolite as the catalyst for fluid catalytic cracking (11, 19). However, this possibility has been hindered due to excessive carbon deposition and limited hydrothermal stability. An additional difficulty was that the pore size could be considerably smaller than the interlayer spacing calculated from XRD (X-ray diffraction). For Zr–PILC, the *interpillar* spacings in the range of 4–8 Å were the limiting pore sizes although XRD results showed an interlayer spacing of 14.6 Å (20, 21). Besides FCC, PILCs have been studied for catalyzing alcohol dehydration (22, 23), alkylation, and other acid catalyzed reactions (23–25). A pillared titanium phosphate was used as the support, for V_2O_5 for the SCR reaction (26).

Despite many studies on the acid sites on PILCs, the nature and properties of these sites are not well understood (11, 14, 27, 28). The acidity and acid site types (Brønsted or Lewis) depend on the exchanged cations, the preparation method, and the starting clay. Both Lewis and Brønsted acid sites exist on pillared clays, with a larger proportion being Lewis acid sites. Our discussion will be focused on the Brønsted acidity because of its importance to the SCR reaction. Two sources for Brønsted acidity have been discussed in the literature. One derives from the structural hydroxyl groups in the clay layer (27). The most likely proton site for some smectites (e.g., montmorillonite) is located at the Al(VI)–O–Mg linkage, where Al(VI) is the octahedrally

[1] To whom correspondence should be addressed.

0021-9517/95 $6.00

coordinated Al and Mg has substituted an Al in the octahedral layer. For other clays, e.g., beidellite and saponite, the proton sites are located at the Si–O–AlOH– groups resulting from isomorphous substitution of Si by Al in the tetrahedral layer. Another likely source for protons derives from the cationic oligomers which upon heating decompose into metal oxide pillars and liberate protons. It has been reported in many studies that both Lewis and Brønsted acidities decrease with temperature of calcination (14, 27). The disappearance of Brønsted acidity is attributed to the migration of protons from the interlayer surfaces to the octahedral layer within the clay layer where they neutralize the negative charge at the substitution atoms (such as Mg) (29). However, of particular significance to our study on the SCR reaction is the fact that upon exposure to NH_3 the migration can be reversed so the proton is again available on the surface (29, 30). Although the total acidity appears to vary with the kind of metal oxide inserted as pillars (27), Brønsted acidity appears to be insensitive to the kind of metal oxide pillars so far used (35).

A potential major advantage of pillared clays for SCR application is their resistance to poisoning. The chemistry of poisoning of the Brønsted acid sites is reasonably well understood (4). However, a significant contributor to catalyst poisoning is apparently the deposition of As_2O_3 and other vapor species within the pore structure of the vanadia catalyst. This problem can be alleviated by a new catalyst design by Hegedus and co-workers (31), which consists of a bimodal pore size distribution in the V_2O_5/TiO_2–SiO_2 catalyst: one group of pores are of the order of micrometers (macropores) and the other group are of the order of angstroms (micropores). The poisonous vapor species in the flue gas such as As_2O_3 deposit on the walls of the macropores due to their low diffusivities. Since the macropores serve as feeder pores to the micropores, they provide the function as filters of poisons. The pore structure of any catalysts made of pillared clays would be unavoidably bimodal. The commercially available clays such as montmorillonite are of particle sizes of micrometers or fraction of a micrometer. A pelletized (or washcoat) PILC catalyst will contain feeder (or poison filter) pores in the interparticle spaces, whereas the intraparticle micropores contain the active catalyst surface for the SCR reaction.

Another class of pillared clays, termed "delaminated clays," was first synthesized by Pinnavaia *et al.* (32). These PILCs are prepared with the same procedures except that freeze drying is used instead of air drying after the ion exchange step. Alumina and chromia clays have been made in this manner. These clays do not exhibit long-range layer stacking as shown by the absence of the 001 X-ray reflections. However, it is believed that short-range stacking with pillared structure still exists, and the overall structure is described as a "house of cards." These clays contain both micropores and macropores (33). The introduction of macropores can significantly increase the diffusion rates, hence the overall activities are increased (as well as altering product distribution in hydrocarbon cracking (19, 32–35)).

EXPERIMENTAL

Experimental apparatus and rate measurement. The reactor system for the SCR reaction was the same as described elsewhere (6). The reactor consisted of a quartz tube. The heating element was a coiled Nichrome wire. The reactor temperature was controlled by an Omega (CN-2010) programmable temperature controller. The catalyst, typically 0.4 g, was supported on a fritted support.

Two sets of flow meters were employed for blending a synthetic flue gas. Rotameters were used to control flows with high flow rates (i.e., N_2, $NH_3 + N_2$, and $NO + N_2$). Mass flow meters were used for gases with low flow rates (SO_2 and O_2). The premixed gases (0.8% NO in N_2 and 0.8% NH_3 in N_2) were supplied by Linde Division. Water vapor was generated by passing nitrogen through a heated gas-wash bottle containing distilled water. To prevent the deposition of ammonium sulfate, the tubings were heated by tapes. NO concentration was continuously monitored by a chemiluminescent NO/NO_x analyzer (Thermo Electron Corporation, Model 10). To avoid any analytical error caused by oxidation of ammonia in the converter of the NO/NO_x analyzer, an ammonia trap (phosphoric acid solution) was installed before the sample inlet.

The absence of intrapellet mass transfer resistance under the experimental conditions has been discussed previously (4), achieved by minimizing the pellet size. The size range for the catalyst was 100–150 US mesh. However, the intracrystalline diffusion resistance was clearly present.

Syntheses of pillared clays. The general method for PILC synthesis is given first, and will be followed by details for the syntheses of the specific pillared clays used in this study. The first step in PILC synthesis is preparation and aging of the pillaring solution to form oligomers. The pillaring agent undergoes hydrolysis, polymerization, and complexation with anions in the solution (13, 15). The hydrolysis conditions are important to the formation of PILC: temperature, pH, and aging time.

Synthesis of delaminated pillared clay. The clay suspension solution was prepared by dispersing 10 g of bentonite (Fisher Scientific, purified grade) in 1 liter distilled water. Our chemical analysis showed that the bentonite

from Fisher was mostly Na^+ montmorillonite. The pillaring agent was prepared by hydrolysis of 3 liters of 0.2 *M* $Fe(NO_3)_3$, and anhydrous sodium carbonate was added to the vigorously stirred $Fe(NO_3)_3$ solution to adjust the pH value of the solution. CO_2 evolution occurred during hydrolysis. The resulting solution was aged for 24 h at room temperature prior to use. The ratio of base to iron was equal to 2, i.e., $OH^-/Fe = 2$, and the final pH value of the solution was 1.8. The aqueous clay suspension was dropwise added to the polyoxoiron cation solution through a funnel. The cation exchange capacity of the bentonite was 103 meq/100 g. The ratio of Fe/clay was approximately 60 (mmole of Fe)/(meq of clay). The pillaring/delaminating (ion exchange) reaction took place at room temperature. It was found that the nature of the pillared clay product depended on the reaction condition. Pillared clay resulted from short (e.g., below 3 h) reaction times at near ambient temperature, whereas delaminated pillared clay formed after long reaction times (e.g., over 12 h) and at higher temperatures (40–50°C). The delamination could be caused by chemical interactions between the pillaring agent and the clay resulting in the breakdown of the clay texture. The delamination process is, however, not understood and is under further study. Both Fe_2O_3–PILC and delaminated Fe_2O_3–PILC were prepared and were subsequently subjected to SCR activity tests. After the reaction, the suspension solution was kept still to separate the top portion of the clear solution. The pillared/delaminated clay was separated by vacuum filtration of the suspension solution. The collected solid sample was redispersed and washed in distilled water. The final sample was collected after dispersion/washing/filtration was repeated three times. The collected solid samples were first dried at 120°C for 24 h, then crushed and sieved to collect the desired fractions. The samples were further heated to 400°C at a rate of 2°C/min in a tubular reactor and were kept at this temperature for a period of at least 12 h. After these pretreatments, the samples were ready for further experiments.

Chemical composition analysis. The chemical composition of the delaminated pillared clay was analyzed by inductively coupled plasma atomic emission spectrometer (Thermo Jarrel Ash 61 ICAP). A fusion–dissolution method was used for sample preparation. The clay sample (0.1 g) was fused with a mixture (0.6 g total) of lithium metaborate and lithium tetraborate (at a weight ratio of 1 : 2) in a graphite crucible at 1000°C for about 1 h. After slowly cooling to room temperature, the fluxed bead was dissolved in 250 ml hot 2% HNO_3 solution. When the fluxed bead dissolved completely, the solution was filtered to remove graphite fiber impurity that came from the crucible. The bentonite sample was analyzed by the same procedure.

In situ infrared spectra. IR spectra were measured with a Nicolet Impact 400 FTIR spectrometer. The samples were pressed into self-supporting disks. The typical weight of the prepared disks was 60–70 mg, which was equivalent to 12–14 mg/cm^2. The *in situ* IR spectra of NH_3 adsorbed on pillared/delaminated clays were recorded by using an IR cell that allowed the sample to be treated at high temperatures under vacuum or in different gases. The samples were pretreated at 300°C *in vacuo* for 2 h prior to adsorption.

X-ray diffraction characterization. X-ray diffraction patterns were obtained using powder samples in a Stoe transmission powder diffractometer with Cu$K\alpha$ radiation. Normally, the data were collected in 2 min. For samples that had weak signals or that were amorphous, the data collection time was extended to at least 6 min.

XRD was also used to determine the Fe_2O_3 particle size. The particle size measurement was based on X-ray line broadening using a method described by Klug and Alexander (36). Silicon was used as a standard for calibration of half-height line width.

Mössbauer spectra. Transmission Mössbauer spectra were measured using a constant acceleration mode Mössbauer spectrometer with ^{57}Co source at room temperature. The catalyst pellets were ground into a powder and were dispersed and mounted on scotch tape to provide a sample diameter of 25 mm. Spectra are reported relative to iron foil.

BET surface area and molecular probing for pore sizes. BET surface areas were measured by adsorption of nitrogen at 77 K using a Quantasorb sorption system.

Thermogravimetric analysis (TGA) was employed to measure the weight gains, by sorption of molecules with known dimensions. Pore volumes for different pore dimensions were measured in this manner.

RESULTS AND DISCUSSION

Chemical Compositions and BET Areas

Inductive coupled argon plasma spectrometric method (ICP) was used for chemical composition analyses. Because of the existence of sodium in the clay samples, sample preparation was done by fusion with lithium borate followed by dissolution for ICP analyses (37). The ICP results are shown in Table 1. The water contents in Table 1 were obtained separately by TGA by heating in helium to 400°C.

Table 1 shows that after ion exchange/pillaring reaction the contents of the cations, Na^+, K^+, Ca^{++}, and Mg^{++}, decreased. However, the most significant change in the synthesized samples was the iron oxide content, which increased from 3.66 to 30.61%. The iron oxide

TABLE 1

Chemical Compositions (wt.%) and BET Surface Areas of Clay and Pillared Clays

	Montmorillonite	Delaminated Fe_2O_3–PILC	Fe_2O_3–PILC
SiO_2	60.32	44.36	59.19
Al_2O_3	19.14	13.93	19.63
Fe_2O_3	3.66	30.61	9.55
TiO_2	0.16	0.15	0.18
CaO	1.41	0.55	0.47
MgO	2.35	1.56	2.06
Na_2O	2.88	0.59	0.65
K_2O	0.51	0.33	0.34
H_2O	8.50	3.54	3.06
Total	98.93	95.61	95.13
BET Surface Area (m^2/g)	24	155	212

pillared clay contained about 10% iron oxide. The larger amount of iron oxide in delaminated/pillared clay was the result of the interactions between the clay and the pillaring solution at higher temperatures and for a longer time. These surface iron oxide particles were further analyzed by XRD and Mössbauer measurements.

BET surface area measurements showed that the BET area of the pillared/delaminated clay increased from 24 to 155 m^2/g whereas that of the Fe_2O_3–PILC increased from 24 to 212 m^2/g. These BET surface areas are consistent with the range of typical values for Fe_2O_3–PILC of 125–324 m^2/g (75). The low value of the pillared/delaminated clay could be caused by the supported iron oxide particles blocking some of the pores.

Structural Analysis by X-Ray Diffraction

X-ray diffraction (powder) patterns of the starting clay (bentonite) are shown in Fig. 1. Figure 1A shows a pattern recorded without pretreatment. Figure 1b shows a pattern recorded after the sample was calcined at 300°C for 2 h. The decrease of d_{001} spacing from 12.1 to 9.85 Å was due to dehydration of the interlayer hydrates.

XRD patterns of smectite clays generally show basal 001 reflection and two dimensional diffraction *hk* only (38, 39). Other *hkl* reflections are usually not observed. The random or unoriented clay sample only shows a strong 001 diffraction; the *hk* diffractions are also strong but diffusive (Fig. 1). Characteristic of the *hk* diffractions is that the peak terminates steeply on the low-angle side but falls off gradually on the high-angle side. The *hk* reflections are characteristic of the type of the clay mineral, whereas the (001) basal reflection is characteristic of the conditions, i.e., interlayer water, cations, etc.

Other major peaks in Fig. 1 are assigned as follows (40, 41). The peaks at 2θ of 19.6° (d = 4.49 Å) and 34.9° (d = 2.57 Å) are assigned to the two-dimensional diffraction, *hk*, reflections. These nonbasal *hk* two-dimensional reflections arise from the diffraction of the random stacking of layers. Each observed *hk* reflection is the summation

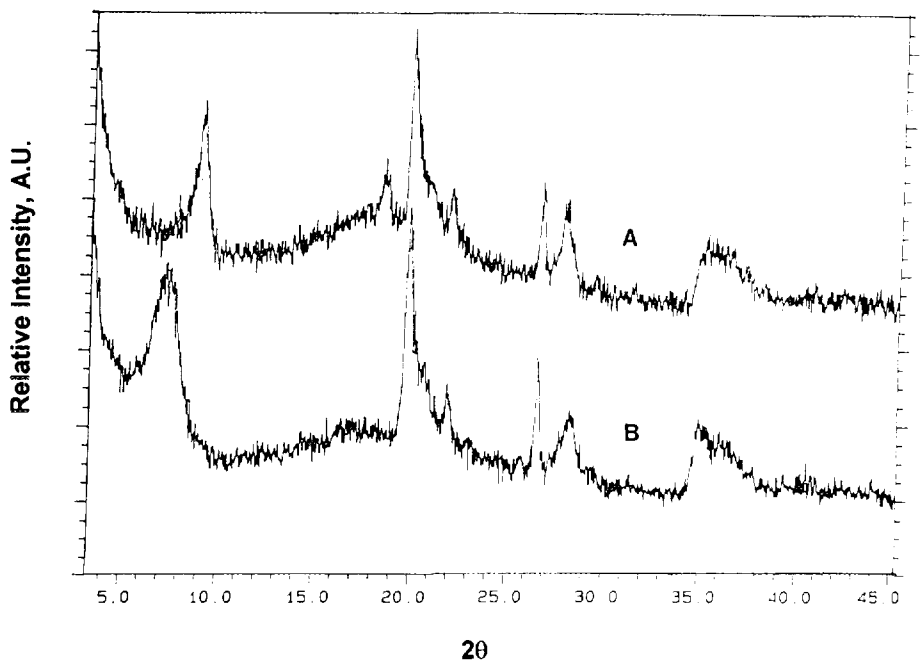

FIG. 1. XRD patterns of bentonite (Cu$K\alpha$ source). (A) No pretreatment; (B) calcined at 300°C for 2 h.

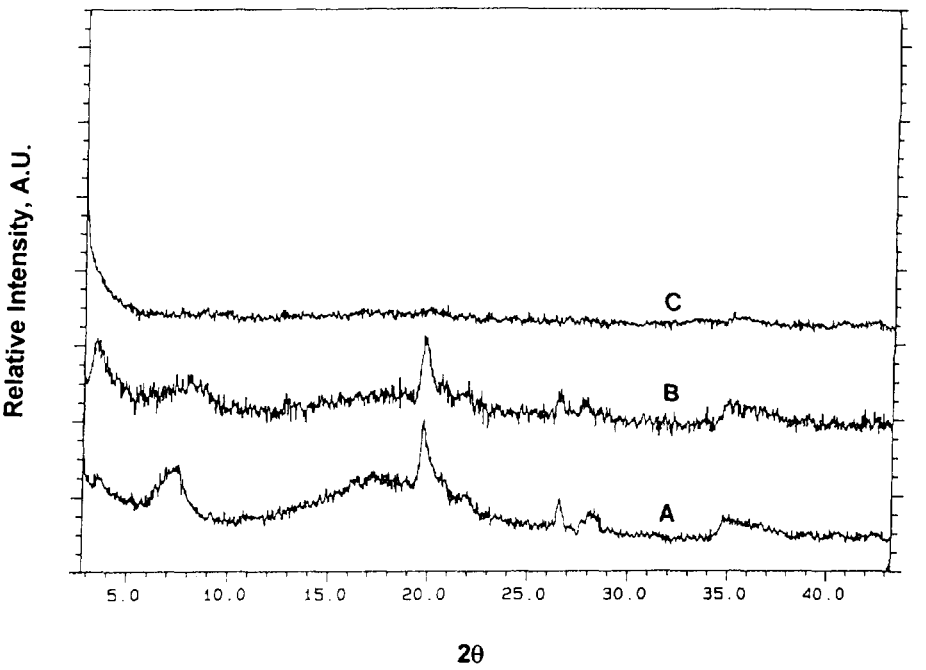

FIG. 2. XRD patterns (Cu$K\alpha$ source) of bentonite (A), Fe_2O_3-pillared clay (B), and delaminated pillared clay (C).

of several *hk* index pairs. The diffraction at 19.6° (d = 4.49 Å) is the summation of *hk* indices of (02) and (11), and the diffraction at 34.9° (d = 2.57 Å) is the summation of *hk* indices of (13) and (20). The two-dimensional *hk* reflections are strongest in unoriented crystals. The peak at 2θ = 26.5° (d = 3.36 Å) is the diffraction of (101) from quartz impurity.

The XRD patterns of the synthesized clay catalysts are shown in Fig. 2. In the Fe_2O_3–pillared clay sample, the d_{001} spacing was 26.4 Å and the two-dimensional *hk* reflections remained. For the delaminated sample, no reflections were observed in the 2θ range 3–45°. The disappearance of the regular basal spacing of clay and the distinct lines corresponding to larger interlayer spacing (i.e., $2\theta < 5°$) was also observed by Burch and Warburton (42) in their preparation of Fe_2O_3 pillared clay. Pillared clays that exhibit no (001) reflection have been referred to as "delaminated clay" (14, 32) in the literature.

The XRD analysis showed that the delaminated sample lost not only its (001) diffraction, but also the two-dimensional diffraction peaks at d-pacings equal to 4.49 and 2.57 Å; i.e., the clay lost its two-dimensional characteristic diffractions. As discussed by Occelli *et al.* (19), the delaminated clay does not preclude the possibility of short-range ordering in the interlayer direction. Also the absence of the two-dimensional reflections does not mean that there was no short-range two-dimensional structure in the clay. Rather, the large two-dimensional structure could have been fragmented into small pieces giving a semi-amorphous form. These small pieces would be the basic units in the structure referred to as a house of cards, which have shown to be superior over the normal pillared clays in many aspects (19, 32, 33, 43, 44).

Micropore Size Distribution by Molecular Probing

The existence of micropores and the micropore size distribution in the delaminated clay sample were further studied by sorption of probe molecules at subcritical temperatures. Under subcritical conditions, micropore filling takes place and the micropore volumes can be calculated (21, 45).

Three probe molecules were used, with their kinetic diameters given below: N_2 (3.6 Å), *n*-hexane (4.9 Å), and 1,3,5-trimethyl benzene (8.6 Å). The cumulative pore volumes were calculated from the equilibrium sorption amount assuming the adsorbate as liquid. The equilibrium sorption amounts of *n*-hexane and trimethyl benzene were measured at room temperature by TGA. The N_2 sorption was measured at 77K with the Quantasorb Analyzer. The results are shown in Fig. 3. For the N_2 sorption, the α_s method was used to obtain the micropore volume (45). From the data shown in Fig. 3, it is seen that a significant amount of micropores with dimensions smaller than 9 Å existed in the delaminated sample. For the Fe_2O_3–pillared clay (21), the cumulative pore volume by N_2 sorption was 0.19 cm^3/g, compared to 0.13 cm^3/g for the delaminated clay. From this result, it is clear that

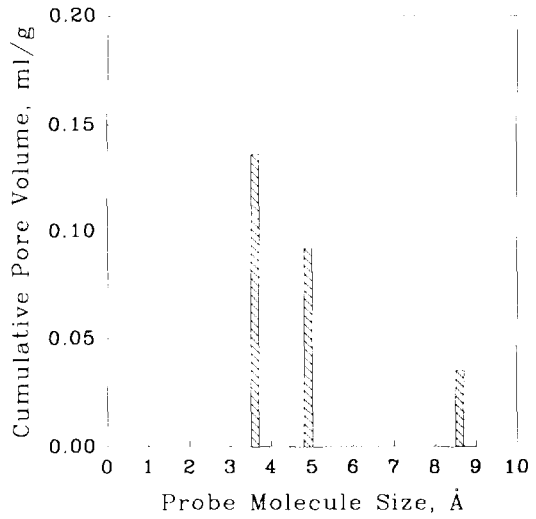

FIG. 3. Cumulative micropore volume as a function of pore dimension measured by micropore filling with probe molecules (N_2 = 3.6 Å, *n*-hexane = 4.9 Å, and 1,3,5-trimethyl benzene = 8.6 Å).

the delaminated sample contained pillared clay fragments, thus it should be properly referred to as *delaminated pillared clay.*

Fe_2O_3 Particle Size by XRD Line Broadening

The chemical composition analysis indicated that there were Fe_2O_3 particles in addition to the fragmented Fe_2O_3–pillared clay. The Fe_2O_3 particle size was analyzed by XRD and Mössbauer spectroscopy.

As discussed, the X-ray diffraction patterns for the clay structure disappeared. However, the weak and broadened peaks at 2θ of 33.36° (d = 2.686 Å) and 35.79° (d = 2.510 Å) became discernible by extending the data collection time to 400 sec, as shown in Fig. 4. These two peaks were reflections by the (104) and (110) faces, respectively, of hematite (46).

From the line broadening, the particle size can be calculated with the formula (36)

$$L = K\lambda/\beta \cos \theta,$$

where L is the mean dimension of the crystallites, K is the Scherrer constant (for spheres, $K = 0.893$ ($\beta_{1/2}$)), λ is the wavelength of Cu$K\alpha$ which is 1.5418 Å, β is the breadth (line width at half height, $\beta_{1/2}$) of the pure diffraction profile on 2θ scale in radians, and θ is the diffraction angle.

The value of β was calculated by the following procedure (36): By using the breadths of silicon standard (b_0) and catalyst sample (B_0) from their XRD profiles and finding the K_α doublet separation of Cu radiation from the literature, the corrected breadths of silicon standard (b) and catalyst sample (B) were obtained. With the ratio of b/B, the β value was found from the curves of correction integral breadths of Debye–Scherrer lines for instrumental broadening. The value of β was found to be 0.6163. Therefore, the average α-Fe_2O_3 particle size was 170 Å.

Characterization of the Delaminated PILC by Mössbauer Spectroscopy

In the case of the delaminated iron pillared clay, there are three distinct sources of iron for the spectra. First, there is the 3.8% iron in the bentonite clay, the Fe_2O_3 pillars, and the larger Fe_2O_3 170-Å particles. Mössbauer spectrum of Wyoming bentonite has appeared in the literature (47), as well as the iron oxide pillared clay (48–50) and the larger Fe_2O_3 particles on SiO_2 (51–54). Ion exchanged iron is not expected due to the calcination step in the preparation of the catalyst (55).

Two spectra of the delaminated iron pillared clay were taken. The first spectrum was taken over the range ±10 mm/sec and is shown in Fig. 5. The magnetically split component was fit to a sextuplet and the superparamagnetic center component was fit to a doublet. Since the superparamagnetic components were difficult to resolve at this velocity range, the second spectrum was taken over the range of ±4 mm/sec and is shown in Fig. 6. The parameters of the sextuplet from Fig. 5 were entered as invariants in the fitting procedure used to fit the spectrum in Fig. 6. As is characteristic of pillared clays (47–50) and other small Fe_2O_3 particles (56), the better resolved superparamagnetic component of the spectrum was fit with two doublets.

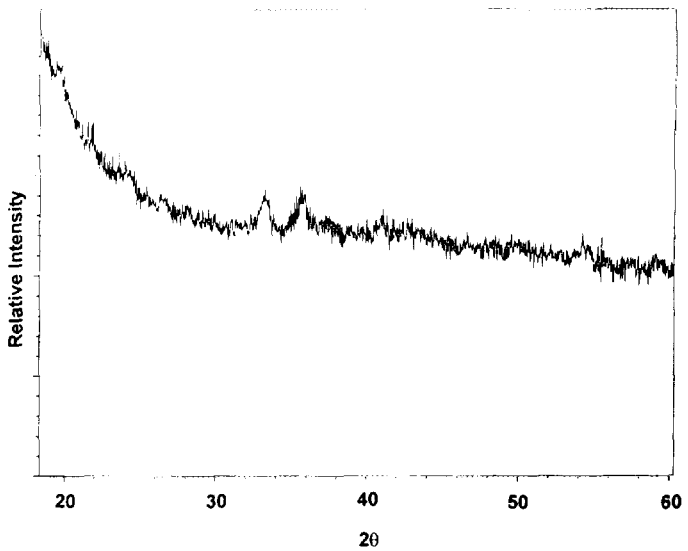

FIG. 4. XRD of the delaminated/pillared clay. The broad and weak peaks at 33.43 and 35.79° are reflections of (104) and (110) faces of hematite.

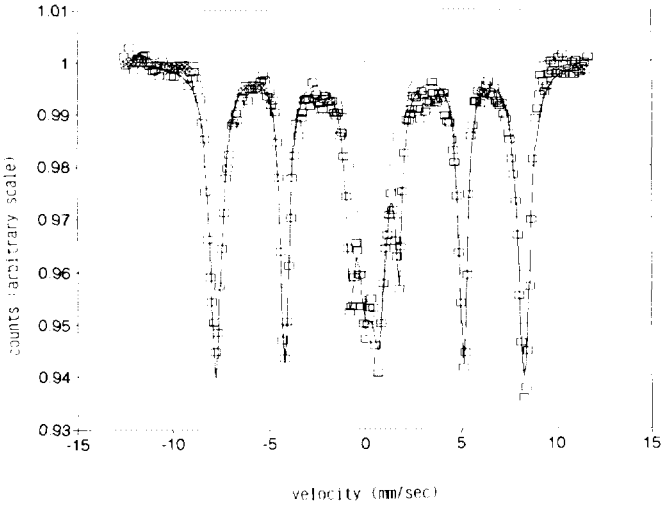

FIG. 5. Mössbauer spectrum of delaminated/pillared clay in the range of ±10 mm/sec.

In the case of the magnetically split sextuplet, only the large 170-Å particles will contribute. The hyperfine splitting was determined to be 500 kOe, which is well below the accepted 515–518 kOe value for bulk Fe_2O_3. The reduction in the hyperfine field is indicative of small iron oxide particles exhibiting magnetic relaxation. This is because the magnetic ordering is temperature and particle volume dependent (51–59). This particle volume dependence can be used to give an estimate of the particle size. From Table 2, it is apparent that the size of the larger Fe_2O_3 particles can be estimated to be about 170 Å, which agrees with the particle size calculations from XRD line broadening. Table 3 gives a summary of the superparamagnetic portion of the spectra reported in Table 2.

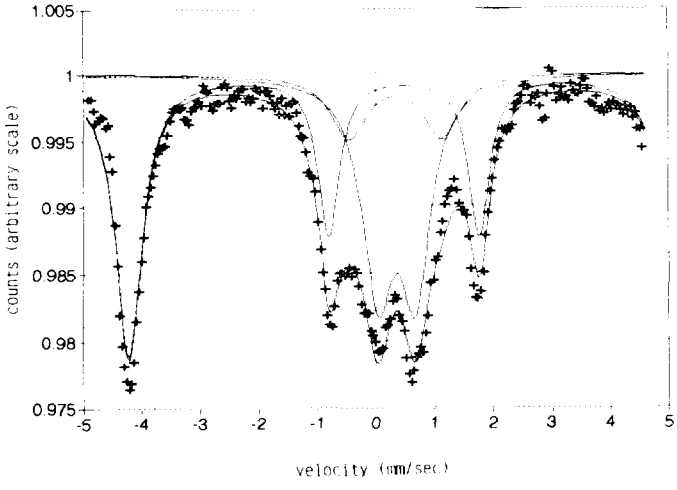

FIG. 6. Mössbauer spectrum of delaminated/pillared clay with best fit (see text).

TABLE 2

The Magnetically Split Component from Fig. 5 Compared to Supported Fe_2O_3/SiO_2 Literature

Hyperfine Field (kOe)	Isomer shift (mm/sec)	Identified species	Reference
496	—	158 Å particles Fe_2O_3/SiO_2	(55)
500	0.38	170 Å particles Fe_2O_3/bentonite	This work (Fig. 5)
503	0.38	180 Å particles Fe_2O_3/SiO_2	(51)
518	0.39	Bulk Fe_2O_3	(51)

The superparamagnetic portion of the spectrum will have contributions from all three of the iron sources. The clay itself contains four different species including Fe^{2+} and hematite (47). No attempt to include Fe^{2+} in the fitted spectrum is made since the doublet due to the Fe^{2+} would be difficult to quantify. The iron oxide pillars will also give a contribution to the superparamagnetic part of the spectra, as well as the superparamagnetic portion of the spectra due to the 170-Å Fe_2O_3 particles. Table 4 reports the two doublets fit from Fig. 6 and compared to other literature values.

All of the iron oxide in the delaminated iron oxide pillared clay was octahedrally coordinated, since the pillars and the larger 170-Å particles were bulk Fe_2O_3 and the Fe^{3+} in the clay itself has been shown to be octahedral (47). Thus, the isomer shift for the two doublets should be at least 0.3 mm/sec (62–64). Several "fitted" spectra of Fig. 6 were discarded because the isomer shift of doublet II was too small. This is consistent with other results (47–52, 56).

It has been suggested that the outer doublet, doublet II, corresponds to the bulk or core quadrupole splitting (49, 56). The surface shell has a larger quadrupole splitting due to the different electric field gradient at the surface when compared to the core. Upon examination of Table 4, one notes that there are large variations in the quadrupole splitting of doublet I. These variations could be due to different amounts of adsorbed water in the pillared clay pores (60, 61).

Upon examining Table 3, it is apparent from the isomer shift and the quadrupole splitting that the superparamagnetic doublet due to magnetic relaxation is contained within doublet II. In addition, Mössbauer spectra of aluminum chlorohydroxide pillared Wyoming bentonite (47) (IS = 0.35, QS = .64) also show that the superparamagnetic portion due to the Fe^{3+} in the clay itself will also be contained in doublet II. Thus, doublet I is a result of pillars in the clay. Typically, doublet I represents about 50% of the Mössbauer spectrum area for iron pillared

TABLE 3

The Superparamagnetic Component from Fig. 5 Compared to Supported Fe_2O_3/SiO_2 Literature

Isomer shift (mm/sec)	Quadrupole splitting (mm/sec)	Superparamagnetic (%)	Identified species	Reference
0.6	0.68	45	158 Å particles Fe_2O_3/SiO_2	(52)
0.34	0.74	29	170 Å particles Fe_2O_3/bentonite	This work (Fig. 5)
0.38	0.44	14[a]	180 Å particles Fe_2O_3/SiO_2	(51)
—	—	0	Bulk Fe_2O_3	(51)

[a] Estimated from Fig. 4 of Ref. (51).

clays (48, 49) so roughly 16% of the relative area in the spectrum may be due to pillars. This is also consistent with results from Kundig *et al.* (51), whose work would suggest that only 10% of the relative area of the spectrum should be superparamagnetic due to 170-Å particles.

Summarizing the characterization results, the structure of the delaminated sample can be described as a house of cards, and a schematic representation of the structure is shown in Fig. 7.

Activity for Selective Catalytic Reduction of NO by NH_3

Our earlier studies showed that Fe_2O_3–pillared clay exhibited a good activity and SO_2 resistance for the NO selective catalytic reduction reaction (6). The NO SCR activities for the delaminated Fe_2O_3–pillared clay were measured under conditions both with and without SO_2/H_2O. The results are shown in Figs. 8 and 9. Three other high-activity catalysts were also included for comparison: V_2O_5 + WO_3/TiO_2, Fe_2O_3/Al_2O_3, and Fe_2O_3/TiO_2. The delaminated pillared clay showed higher activities over the other catalysts under conditions without SO_2/H_2O.

The V_2O_5 + WO_3/TiO_2 contained 8.2% WO_3 and 4.8% V_2O_5. This is a catalyst being commercially used (65, 66). Under reaction conditions without SO_2 and H_2O, as shown in Fig. 8, the delaminated Fe_2O_3–PILC showed the highest activities at all temperatures. Under conditions with both SO_2 and H_2O, however, the delaminated Fe_2O_3–PILC exhibited inhibition effects, as shown in Fig. 9. The SO_2/H_2O inhibition was reversible, i.e., the activity recovered upon termination of H_2O/SO_2, as shown in Table 5. Also, the inhibition effect decreased with increasing temperature as shown in Fig. 9.

From the conversion data and the reaction conditions, one may calculate the rate constants. For a plug-flow integral reactor, for first-order (with respect to NO) reaction (which was the case), and under diffusion resistance free condition (which was nearly the case in our reaction system, Chen and Yang (65)), the rate constant k is given by

$$k = -\frac{F_0}{[NO]_0 W} \ell n(1 - X),$$

TABLE 4

The Superparamagnetic Component from Fig. 6 Compared to Literature

Doublet I: Isomer shift (mm/sec)	Doublet I: Quadrupole splitting (mm/sec)	Doublet I: Relative area (%)	Doublet II: Isomer shift (mm/sec)	Doublet II: Quadrupole splitting (mm/sec)	Doublet II: Relative area (%)	Reference
0.33	1.58	8	0.35	0.64	21	This work (Fig. 6)
0.3	1.29	29	0.33	0.74	68	(49)
0.33	0.93	49	0.34	0.54	51	(48)
0.33	0.9	45	0.35	0.54	55	(48)
—	—	—	0.37	0.76	100	(50)

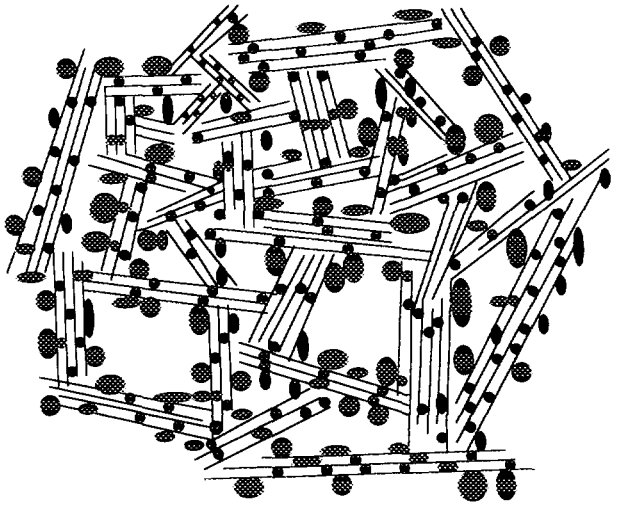

FIG. 7. Schematic representation of the delaminated/pillared clay containing iron oxide particles.

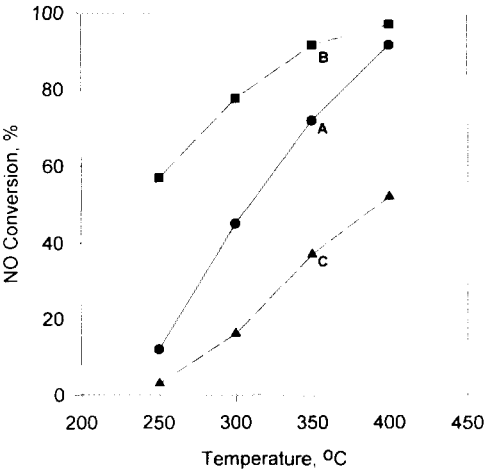

FIG. 9. Selective catalytic reduction of NO with NH_3 on different catalysts. Reaction conditions are the same as in Fig. 8 except H_2O (8%) and SO_2 (500 ppm) are added. (A) Delaminated pillared clay, (B) V_2O_5 + WO_3/TiO_2, and (C) Fe_2O_3-pillared clay.

where F_0 is the molar NO feed rate, $[NO]_0$ is the molar NO concentration at the inlet (at the reaction temperature), W is the catalyst amount, and X is the fractional NO conversion. The catalyst amount W is expressed in grams rather than in surface area or active sites, since the true surface area (which is not the BET N_2 area for microporous materials) and active sites are not known for our catalysts and no surface area information was given for the supported Fe_2O_3 catalysts. From Fig. 8, the values of k (in $cm^3/g/s$) are (for catalysts A to E):

At 350°C: 137(A), 125(B), 40(C), 22(D), and 15(E).

At 400°C: 176(A), 161(B), 53(C), 30(D), and 18(E).

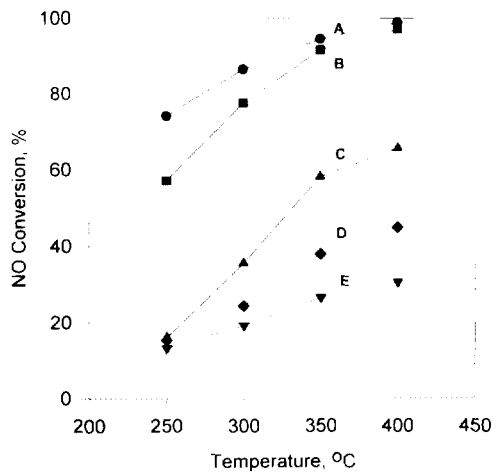

FIG. 8. Selective catalytic reduction of NO with NH_3 on different catalysts. Reaction conditions: NO = NH_3 = 1000 ppm, O_2 = 2%, N_2 balance, total flow rate = 500 ml/min, catalyst weight = 0.4 g. (A) Delaminated pillared clay, (B) V_2O_5 + WO_3/TiO_2, (C) Fe_2O_3-pillared clay, (D) Fe_2O_3/Al_2O_3, and (E) Fe_2O_3/TiO_2.

Supported Fe_2O_3 catalysts were among the most active catalysts for the NO SCR reaction (67). The data of Wong and Nobe were also included for comparison, Fig. 8, and the rate constants are given above as catalysts D and E. Wong and Nobe only studied the reaction without SO_2 and H_2O, and their reactant gas composition was the same as that used in this study. Their catalyst amount was 14 g and the gas flow rate was 300 liter NTP/h. So a conversion, based on first-order reaction (67) and plug-flow reactor, was needed for our comparison. The conversions shown in Fig. 8 were compared with this conversion by using the equation above. It is seen that the two supported Fe_2O_3 catalysts show lower activities than Fe_2O_3–pillared clay, as well as the other catalysts. It was further noted by Wong and Nobe that there was pore diffusion limitation in their reactions, and effectiveness factors ranging from 16% to 95% were indicated. By including the effectiveness factors, however, the NO conversion for the delaminated pillared clay was still higher than the supported Fe_2O_3 catalysts.

The stability of iron oxide pillared clays have been studied by a number of researchers. It was reported that

TABLE 5

Longevity Test of SCR Activity for the Delaminated Fe_2O_3 Pillared Clay

Time (h)	2[a]	3	24	48	96	97[a]
NO conversion (%)	97.5	84.0	83.0	85.0	84.5	98.8

Note. Reaction conditions: NO = NH_3 = 1000 ppm, O_2 = 2%, SO_2 = 1000 ppm (when used), H_2O = 8% (when used), total flow rate = 500 ml/min, catalyst = 0.4 g, 400°C.

[a] Reaction without water vapor and SO_2.

sulfite–pillared clay was stable at elevated temperatures and pressures and iron oxide pillared clay was stable under reducing conditions even at a temperature as high as 500°C (68). However, unstable iron oxide pillared clays have also been observed. Scanning electron microscopy/energy dispersive spectroscopy (SEM/EDS) analysis (25) showed that the iron oxide pillars migrated to the edge of the clay when the pillared clay was exposed to air at ambient temperature for three months. Prompted by these reports, the delaminated pillared clay was subjected to a longevity test under the SCR conditions. As shown in Table 5, the NO conversion stayed in the range 83–86% when SO_2 and H_2O were switched on, and the conversion was stable at 95–98% without SO_2 and H_2O. No deactivation was shown after 4 days. The delaminated clay is therefore stable under the SCR reaction conditions.

FTIR Characterization

To examine the surface acidity and to identify the Brønsted and Lewis acid sites of the delaminated/pillared clay, FTIR spectra of adsorbed ammonia were measured. The spectra of adsorbed ammonia at room temperature are shown in Fig. 10.

Figure 10 shows the effects of water vapor on the absorption bands at 1636.7, 1458, and 1595.1 cm^{-1}. The peak at 1636.7 cm^{-1} is attributed to the bending vibration of surface hydroxyl groups (69). All spectra were taken in the transmission mode and were obtained as the ratios of the spectra after adsorption against the spectra before adsorption. In the background spectrum, a strong absorption band for the surface hydroxyl at 1636.7 cm^{-1} appeared (not shown in Fig. 10). When NH_3 was introduced, it interacted with the surface hydroxyl groups forming NH_4^+, which resulted in the strong band at 1456.9 cm^{-1}. Therefore the negative absorption bands in Figs. 10a and 10b were due to the consumption of surface hydroxyl groups by ammonia adsorption, since all spectra were obtained as the ratios against that of the sample before NH_3 exposure. Similar negative peaks were also observed when ammonia was adsorbed on V_2O_5/SiO_2 (2). The strong peak at 1458 cm^{-1} was due to ammonia adsorbed on Brønsted acid sites (70). The weak peak at 1595.1 cm^{-1} was likely due to ammonia coordinatively adsorbed on the catalyst surface, i.e., on Lewis acid sites.

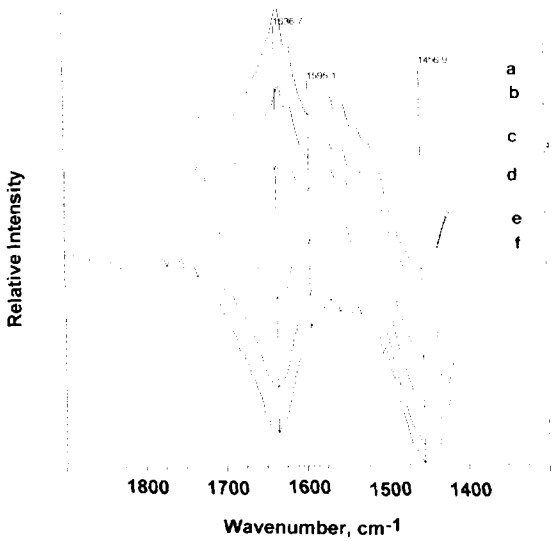

FIG. 10. FTIR spectra (transmittance) of ammonia adsorbed on delaminated Fe_2O_3 pillared clay (a). (b)–(f) are after exposure to 2% H_2O, at 1-min successive time intervals. All spectra are taken at room temperature and are obtained as ratios against the spectrum before NH_3 exposure (but after calcination).

Figure 10 shows the effects of water vapor on the absorption bands at 1636.7, 1458, and 1595.1 cm^{-1}. The peak at 1636.7 cm^{-1} is attributed to the bending vibration of surface hydroxyl groups (69). All spectra were taken in the transmission mode and were obtained as the ratios of the spectra after adsorption against the spectra before adsorption. In the background spectrum, a strong absorption band for the surface hydroxyl at 1636.7 cm^{-1} appeared (not shown in Fig. 10). When NH_3 was introduced, it interacted with the surface hydroxyl groups forming NH_4^+, which resulted in the strong band at 1456.9 cm^{-1}. Therefore the negative absorption bands in Figs. 10a and 10b were due to the consumption of surface hydroxyl groups by ammonia adsorption, since all spectra were obtained as the ratios against that of the sample before NH_3 exposure. Similar negative peaks were also observed when ammonia was adsorbed on V_2O_5/SiO_2 (2). The strong peak at 1458 cm^{-1} was due to ammonia adsorbed on Brønsted acid sites (70). The weak peak at 1595.1 cm^{-1} was likely due to ammonia coordinatively adsorbed on the catalyst surface, i.e., on Lewis acid sites.

Figure 10 shows that the IR band at 1637 cm^{-1} changed from a negative one to a positive one after about 3 min of exposure to 2% H_2O. It is interesting to note that the peak intensity at 1458 cm^{-1} actually increased in the first few minutes upon H_2O exposure. Concurrently, the weak band at 1595 cm^{-1} gradually decreased and eventually disappeared. This suggests that, with the addition of water vapor, the Lewis acid sites were converted to Brønsted acid sites and the coordinatively adsorbed ammonia was transformed into ammonium ions on the surface.

For clays and their variants, the surface acidity and the type of acid sites (Brønsted or Lewis sites) are dependent on the extent of hydration–dehydration. The FTIR spectrum of ammonia absorbed on the delaminated/pillared clay at 150°C is shown in Fig. 11. A very strong and sharp

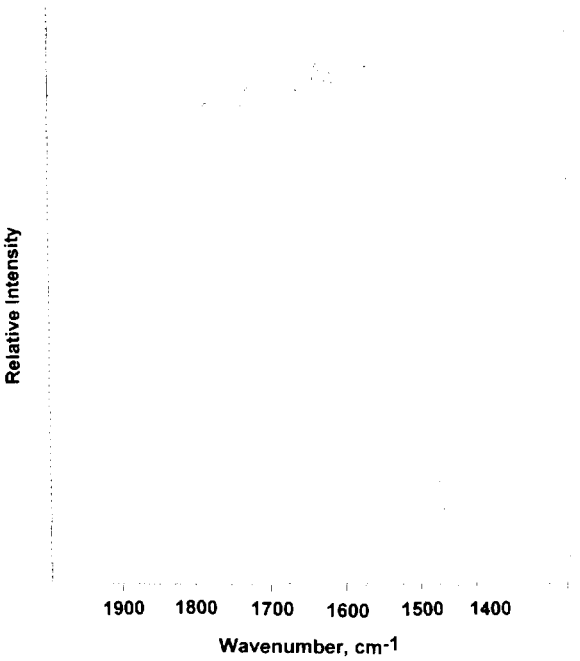

FIG. 11. FTIR spectra (transmittance) of ammonia adsorbed on delaminated/pillared clay at 150°C.

peak at 1453 cm^{-1} was observed. The difference with the spectra taken at room temperature was that there was no negative band at around 1630 cm^{-1}. This was due to dehydration at 150°C which eliminated the adsorbed water molecules.

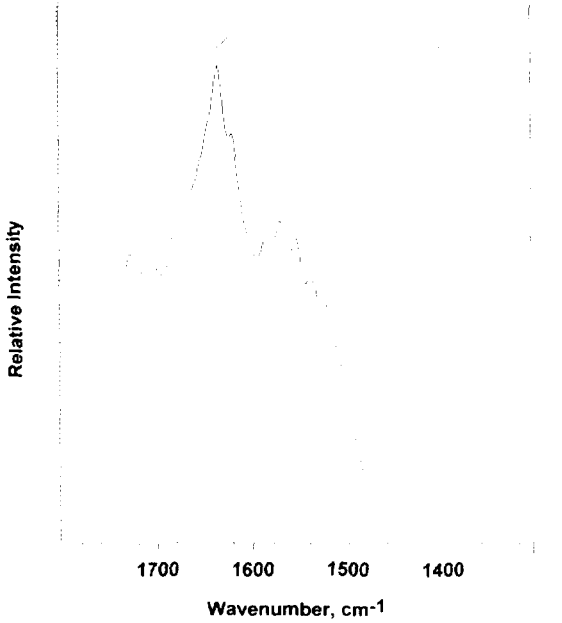

FIG. 12. FTIR spectra (transmittance) of ammonia adsorbed on montmorillonite (top) and ammonia adsorbed on delaminated/pillared clay (bottom) at room temperature.

The IR results showed that the delaminated/pillared clay was abundant in Brønsted acid sites on the surface. As shown in our previous work (4, 65, 71, 72) Brønsted acid sites on V_2O_5 and other oxides are the active sites for selective catalytic reduction of NH_3 with NO. The high catalytic activity for SCR of this clay catalyst may be correlated with its strong Brønsted acidity.

Figure 12 shows the IR spectra of ammonia adsorbed on montmorillonite and the delaminated/pillared clay on the same intensity scale. Ammonia adsorbed on montmorillonite also gave an absorption band at around 1450 cm^{-1}, but its relative intensity was low. It is known that there are only Lewis acid sites on Fe_2O_3 (73, 74). The origin of the strong Brønsted acid sites in this clay catalyst was probably the result of the interactions between Fe_2O_3 and the clay. Further studies of these interactions are in progress.

ACKNOWLEDGMENTS

This work was supported by the Department of Energy under Grant DE-FG22-93PC932217. We thank the Editor, Professor Delgass, for helpful comments on Mössbauer analysis, and Professor Carl Lund for using his Mössbauer spectrometer and for discussion.

REFERENCES

1. Bosch, H., and Jassen, F., *Catal. Today* **2,** 369 (1988).
2. Rajadhyaksha, R. A., and Knözinger, H., *Appl. Catal* **51,** 81 (1989).
3. Rajadhyaksha, R. A., Hausinger, G., Zeilinger, H., Ramstetter, A., Schmelz, H., and Knözinger, H., *Appl. Catal.* **51,** 67 (1989).
4. Chen, J. P., and Yang, R. T., *J. Catal.* **125,** 411 (1990).
5. Topsøe, N. Y., *J. Catal.* **128,** 499 (1991).
6. Yang, R. T., Chen, J. P., Kikkinides, E. S., Cheng, L. S., and Cichanowicz, J. E., *Ind. Eng. Chem. Res.* **31,** 1440 (1992).
7. Brindley, G. M., and Sempels, R. E., *Clays Clay Miner.* **12,** 229 (1977).
8. Vaughan, D. E. W., Lussier, R. J., and Magee, J. S., U.S. Patent 4,176,090, 1979.
9. Lahav, N., Shani, N., and Shabtai, J., *Clays Clay Miner.* **26,** 107 (1978).
10. Loeppert, R. H., Mortland, M. M., and Pinnavaia, T. J., *Clays Clay Miner.* **27,** 201 (1979).
11. Occelli, M. L., and Tindwa, R. M., *Clays Clay Miner.* **31,** 22 (1983).
12. Pinnavaia, T. J., *Science* **220,** 365 (1983).
13. Burch, R., *Catal. Today* **2,** 185 (1988).
14. Figueras, F., *Catal. Rev. Sci. Eng.* **30,** 457 (1988).
15. Baes, C. F., and Mesmer, R. E., "The Hydrolysis of Cations," Wiley, New York, 1976.
16. Clearfield, A., *NATO Adv. Study Inst. Ser., Ser. C* **231,** 271 (1988).
17. Drezdon, M. A., *Inorg. Chem.* **27,** 4628 (1988).
18. Sprung, R., Davis, M. E., Kauffman, J. S., and Dybowski, C., *Ind. Eng. Chem. Res.* **29,** 213 (1990).
19. Occelli, M. L., Landau, S. D., and Pannavaia, T. J., *J. Catal.* **90,** 256 (1984).
20. Yang, R. T., and Baksh, M. S. A., *AIChE J.* **37,** 679 (1991).
21. Baksh, M. S. A., Kikkinides, E. S., and Yang, R. T., *Ind. Eng. Chem. Res.* **31,** 2182 (1992).
22. Burch, R., and Warburton, C. I., *J. Catal.* **97,** 511 (1986).
23. Occelli, M. L., Innes, R. A., Hwu, F. S. S., and Hightower, J. W., *Appl. Catal.* **14,** 69 (1985).

24. Occelli, M. L., Hsu, J. T., and Galya, L. G., *J. Mol. Catal.* **33,** 371 (1985).
25. Rightor, E. G., Tzou, M. S., and Pinnavaia, T. J., *J. Catal.* **130,** 29 (1991).
26. Czarnecki, L. J., and Anthony, R. G., *AIChE J.* **36,** 794 (1990).
27. He, M. Y., Liu, Z., and Min, E., *Catal. Today* **2,** 321 (1988).
28. Jones, W., *Catal. Today* **2,** 357 (1988).
29. Tennakoon, D. T., Jones, W., and Thomas, J. M., *J. Chem. Soc., Faraday Trans. 1,* **82,** 3081 (1986).
30. Molinard, A., Peeters, K. K., Maes, N., and Vansant, E. F., "Separation Technology," (E. F. Vansant, Ed.), p. 445. Elsevier, New York, 1994.
31. Beeckman, J. W., and Hegedus, L. L., *Ind. Eng. Chem. Res.* **30,** 969 (1991).
32. Pinnavaia, T. J., Tzou, M-S., Landau, S. D., and Raythatha, R., *J. Mol. Catal.* **27,** 195 (1984).
33. Occelli, M. L., Landau, S. D., and Pinnavaia, T. J., *J. Catal.* **104,** 331 (1987).
34. Pinnavaia, T. J., Tzou, M. S., Landau, S. D., and Raythatha, R. H., *J. Mol. Catal.* **27,** 195 (1984).
35. Occelli, M. L., *Catal. Today* **2,** 339 (1988).
36. Klug, H. P., and Alexander, L. E., "X-Ray Diffraction Procedures—For Polycrystalline and Amorphorous," 2nd ed., Chap. 9. Wiley, New York, 1974.
37. Newman, A. C. D., and Brown, G., *in* "Chemistry of Clay and Clay Minerals." Wiley, New York, 1987; literature cited therein.
38. Klug, H. P., and Alexander, L. E., "X-Ray Diffraction Procedures—For Polycrystalline and Amorphorous," 2nd ed., p. 667. Wiley, New York, 1974.
39. Bailey, S. W., *in* "Structures of Clay Minerals and Their X-Ray Identification" (G. W. Brindley and G. Brown, Eds.), Mineralogical Society Monograph, Vol. 5. Mineralogical Society, London, 1980.
40. Bailey, S. W., *in* "Structures of Clay Minerals and Their X-Ray Identification" (G. W. Brindley and G. Brown, Eds.), Mineralogical Society Monograph, Vol. 5. Mineralogical Society, London, 1980.
41. Mott, C. J. B., *in* "Pillared Clays." (R. Burch, Ed.) Elsevier, Amsterdam; *Catal. Today* **2,** 187 (1988).
42. Burch, R., and Warburton, C. I., *J. Chem. Soc., Chem. Commun.,* 117 (1987).
43. Pinnavaia, T. J., Tzou, M. S., and Landau, S. D., U.S. Patent, 4,665,045, May 12, 1987.
44. Occelli, M. L, Landau, S. D., and Pinnavaia, T. J., *J. Catal.* **104,** 331 (1987).
45. Gregg, S. J., and Sing, K. S. W., "Adsorption, Surface Area and Porosity," 2nd ed. Academic Press, London, 1982.
46. Klug, H. P., and Alexander, L. E., "X-Ray Diffraction Procedures—For Polycrystalline and Amorphous," 2nd ed., p. 371. Wiley, New York, 1974; literature cited therein.
47. Occelli, M. L., Stencel, J. M., and Suib, S. L., *J. Mol. Catal.* **64,** 221 (1991).
48. Martin-Luengo, M. A., Martins-Carvalho, H., Ladriere, J., and Grange, P., *Clay Miner.* **24,** 505 (1989).
49. Doff, D. H., Gangas, N. H. J., Allan, J. E. M., and Coey, J. M. D., *Clay Miner.* **23,** 367 (1988).
50. Lee, W. Y., Raythatha, R. H., and Tatarchuk, B. J., *J. Catal.* **115,** 159 (1989).
51. Kundig, W., Bömmel, H., Constabaris, G., and Lindquist, R. H., *Phys. Rev.* **147** (2), 327 (1966).
52. Hobson, M. C., and Gager, H. M., *J. Catal.* **16,** 254 (1970).
53. Yoshioka, T., Koezuka, J., and Ikoma, H., *J. Catal.* **16,** 264 (1970).
54. Lund, C. R. F., and Dumesic, J. A., *J. Phys. Chem.* **85,** 317 (1981).
55. Helson, J. A., and Goodman, B. A., *Clays Miner.* **18,** 117 (1983).
56. Kundig, W., Ando, K. J., Lindquist, R. H., and Constabaris, G., *Czech. J. Phys.* **B17,** 467 (1967).
57. Topsøe, H., and Boudart, M., *J. Catal.* **31,** 346 (1973).
58. Morup, S., and Topsøe, H., *Appl. Phys.* **11,** 63 (1976).
59. Mørup, S., Dumesic, J. A., and Topsøe, H., "Applications of Mossbauer Spectroscopy" (R. Cohen, Ed.) Academic Press, New York, 1980.
60. Gager, H. M., Hobson, M. C., and Lefelhocz, J. F., *Chem. Phys. Lett.* **15** (1), 124 (1972).
61. Gager, H. M., Lefelhocz, J. F., and Hobson, M. C., *Chem. Phys. Lett.* **23** (3), 386 (1973).
62. Meagher, A., *Zeolites* **9,** 87, (1989).
63. Garten, R. L., Delgass, W. N., and Boudart, M., *J. Catal.* **18,** 90 (1970).
64. Coey, J. M. D., *At. Energy Rev.* **18** (1), 73 (1980).
65. Chen, J. P., and Yang, R. T., *Appl. Catal.* **80,** 135 (1992).
66. Tuenter, G., Leeuwen, W. F. V., and Snepvangers, L. J. M., *Ind. Eng. Chem. Prod. Res. Dev.* **25,** 633 (1986).
67. Wong, W. C., and Nobe, K., *Ind. Eng. Chem. Prod. Res. Dev.* **25,** 179 (1986).
68. Thomas, J. M., and Theocharis, C. R., *in* "Perspectives in Catalysis—Chemistry for the 21st Century," p. 478. Blackwell Scientific Publications, Oxford, 1992.
69. Little, L. H., "Infrared Spectra of Adsorbed Species." Academic Press, London, 1966.
70. Kung, M. C., and Kung, H. H., *Catal. Rev.–Sci. Eng.* **27,** 425 (1985).
71. Chen, J. P., and R. T. Yang, *J. Catal.* **139,** 277 (1993).
72. Chen, J. P., Yang, R. T., Buzanowski, M. A., and Cichanowicz, J. E., *Ind. Eng. Chem. Res.* **29,** 1431 (1990).
73. Rochester, C. H., and Topham, S. A., *J. Chem. Soc., Faraday Trans. 1* **75,** 1259 (1979).
74. Peri, J. B., *J. Phys. Chem.* **69,** 220 (1965).
75. Warburton, C. I., *in* "Pillared Clay" (R. Burch, Ed.); *Catal. Today* **2,** 275 (1988).